

Maximally entangled mixed states: Creation and concentration

Nicholas A. Peters, Joseph B. Altepeter, David A. Branning, Evan R. Jeffrey, Tzu-Chieh Wei, and Paul G. Kwiat
 Physics Department, University of Illinois, 1110 West Green Street, Urbana, IL 61801
 (Dated: July 31, 2003)

Using correlated photons from parametric downconversion, we extend the boundaries of experimentally accessible two-qubit Hilbert space. Specifically, we have created and characterized maximally entangled mixed states that lie above the Werner boundary in the linear entropy-tangle plane. In addition, we demonstrate that such states can be efficiently concentrated, simultaneously increasing both the purity and degree of entanglement.

PACS numbers: 42.50.Dv, 42.65.Lm, 03.67.Mn

By exploiting quantum mechanics it is possible to implement provably secure cryptography [1], teleportation [2], and super-dense coding [3]. These protocols and most others in quantum information processing require a known initial quantum state, and typically have optimal results for pure, maximally-entangled initial states. However, decoherence and dissipation may cause the states to become mixed and/or less entangled. As the success of a protocol such as quantum teleportation often hinges on both the purity and the entanglement of the initial state [4], it is important to study the interplay of these properties. Using a source of 2-qubit polarization states [5], we investigate the creation of maximally entangled mixed states, and their concentration [6, 7].

Maximally entangled states have been demonstrated in a variety of systems [8, 9, 10, 11, 12, 13]. However, there are several classes of entangled states; maximally entangled and nonmaximally entangled pure states [5, 9, 14], nonmaximally entangled mixed states [15], and the special case of Werner states [16] (incoherent combinations of a completely mixed state and a maximally entangled pure state) have all been experimentally realized using optical qubits. For some time it was believed that Werner states were maximally entangled for a given level of mixedness, because their entanglement cannot be increased by local unitary operations. However, Munro et al. [17] discovered a class of states that are more entangled than Werner states of the same purity [18]. These maximally entangled mixed states (MEMS) possess the maximal amount of entanglement (tangle or entanglement of formation) for a given degree of mixedness (linear entropy).

We have experimentally explored the region on the linear entropy-tangle plane above the Werner state line by generating states close to the MEMS boundary [19]. We have also implemented a partial polarizer-based iterative concentration technique which simultaneously increases both the purity and the entanglement, at the cost of decreasing the size of the initial ensemble of photon pairs. Although the implementation requires knowledge of the initial state, we show that MEMS exist where this "Procrustean" iterative technique [6, 20, 21] is much more efficient than other recent entanglement concentration schemes [22, 23].

The exact form of the MEMS density matrix depends on the measures used to quantify the entanglement and mixedness [24]; here we use the tangle ($T(\rho) = \max\{0, \sqrt{1 - 4\text{Tr}(\rho^2)}\}$) [25], i.e., the concurrence squared, and the linear entropy ($S_L(\rho) = \frac{4}{3}[\ln \text{Tr}(\rho^2)]$) [4]. Here λ_i are the square roots of the eigenvalues of $(\rho_1 \rho_2)^\dagger (\rho_1 \rho_2)$, in non-increasing order by magnitude, with $\lambda_2 = \begin{pmatrix} 0 & i \\ i & 0 \end{pmatrix}$. For this parameterization, the MEMS density matrices exist in two subclasses [17], MEMS I and MEMS II, which have two and three eigenvalues, respectively:

$$\text{MEMS I} = \begin{pmatrix} 0 & & & & 1 \\ & \frac{r}{2} & 0 & 0 & \frac{r}{2} \\ & 0 & 1-r & 0 & 0 \\ & 0 & 0 & 0 & 0 \\ & \frac{r}{2} & 0 & 0 & \frac{r}{2} \end{pmatrix}; \quad \begin{pmatrix} 2 \\ 3 \\ r \\ 1 \end{pmatrix}; \quad (1)$$

$$\text{MEMS II} = \begin{pmatrix} 0 & & & & 1 \\ & \frac{1}{3} & 0 & 0 & \frac{r}{2} \\ & 0 & \frac{1}{3} & 0 & 0 \\ & 0 & 0 & 0 & 0 \\ & \frac{r}{2} & 0 & 0 & \frac{1}{3} \end{pmatrix}; \quad \begin{pmatrix} 0 \\ r \\ \frac{2}{3} \end{pmatrix}; \quad (2)$$

where the parameter r is the concurrence of the state.

Our creation of MEMS states involves three steps: creating an initial state of arbitrary entanglement, applying local unitary transformations, and inducing decoherence. First, frequency degenerate 702-nm photons are created by pumping thin nonlinear BBO crystals with a 351-nm Ar-ion laser. Polarization entanglement is realized by pumping two such crystals oriented such that their optic axes are in perpendicular planes. With a pump polarized at θ_1 , a variable entanglement superposition state $\cos \frac{1}{2} \theta_1 |H\rangle |H\rangle + \sin \frac{1}{2} \theta_1 |V\rangle |V\rangle$ is created, where $|H\rangle$ represents two horizontally polarized and $|V\rangle$ two vertically polarized photons [5, 14]. The pump polarization is controlled by a half-wave plate (HW P₁ in Fig. 1) set to $\theta_1 = 45^\circ$.

To create the MEMS I states, we start by setting the initial degree of entanglement to that of the target MEMS. Next a maximum likelihood tomography [14, 27] of this initial entangled state is taken to determine the appropriate settings of HW P₂ and HW P₃ in Fig. 1. These waveplates effectively set the diagonal elements

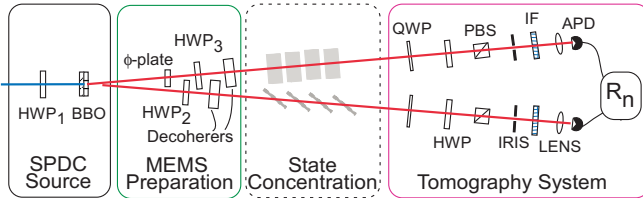


FIG. 1: Experimental arrangement to create, characterize, and concentrate maximally entangled mixed states (MEMS). Half-waveplate HWP_1 sets the initial entanglement of the pure state. The ϕ -plate sets the relative phase between $|H\rangle H_i$ and $|V\rangle V_i$ in the initial state. HWP_2 and HWP_3 rotate the state into the active bases of the decoherers to adjust the amount of entropy. The tomography system uses a quarter-waveplate (QWP), HWP and polarizer to analyze in arbitrary polarization bases; the transmitted photons are counted in coincidence via avalanche photodiodes. The dashed box contains concentrating elements (a variable number of glass slips) oriented at Brewster's angle to completely transmit $|V\rangle V_i$ in the top arm and $|H\rangle H_i$ in the lower arm, but only partially transmit the orthogonal polarization states.

of the density matrix to the target values for the desired MEMS. The initial tomography must be precise, because the waveplate settings are critically dependent on the initial state, as well as on the precise birefringent retardation of the waveplates themselves. After the waveplates, the state passes through decoherers which lower specific off-diagonal elements in the density matrix, yielding the final state. In our scheme, each decoherer is a thick birefringent element (1 cm quartz) chosen to have a polarization-dependent optical path length difference (140 [28]) greater than the downconverted photons' coherence length ($L_c = \frac{c}{2} = 70$ nm), determined by a 10-nm FWHM interference filter placed before each detector, but much less than the coherence length of the pump [29]. The decoherers in each arm couple the polarization with the relative arrival times of the photons. While two horizontal ($|H\rangle H_i$) or two vertical ($|V\rangle V_i$) photons will be detected at the same time, the state $|H\rangle V_i$ will in principle be detected first in arm one and then in arm two, and vice versa for the state $|V\rangle H_i$ (assuming the decoherer slows vertically polarized photons relative to horizontally polarized ones). Tracing over timing information during state analysis then erases coherence between the $|H\rangle V_i$ and $|V\rangle H_i$ terms of the state. A sample tomography of a MEMS I state is shown in Fig. 2(a), first reported in [19]. Note that our decoherence method essentially couples the polarization to the frequency degree of freedom. As recently demonstrated [30], one could instead use the spatial degree of freedom to induce decoherence; however, the states are then not suitable, e.g., for use in fiber optic systems, or where interference methods are needed.)

MEMS II states are created by first producing the MEMS I state at the MEMS I/II boundary, i.e., the state with $r = \frac{2}{3}$. In order to travel along the MEMS

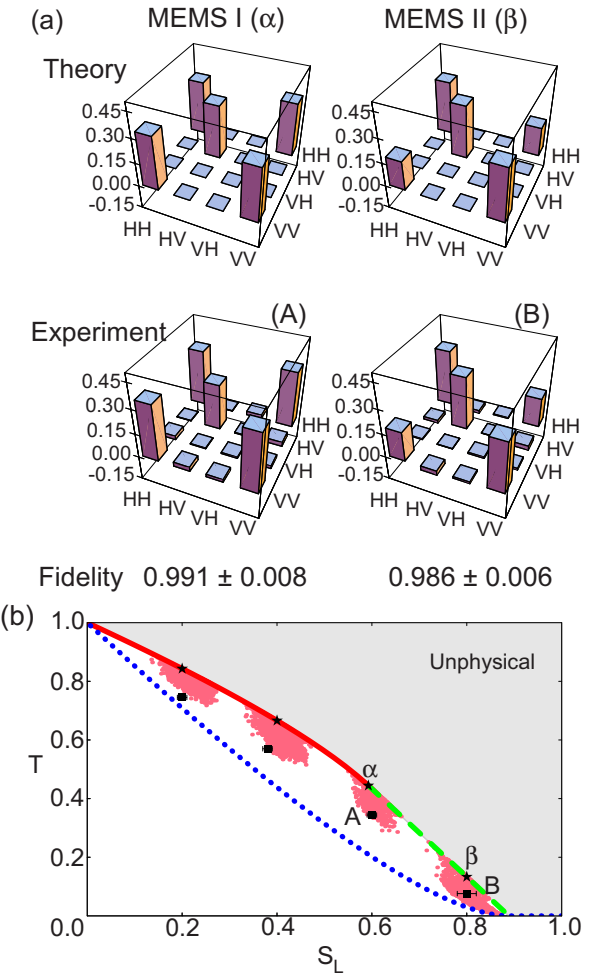


FIG. 2: MEMS data. (a) Density matrix plots of the real components of a MEMS I ($r = \frac{2}{3}$) and a MEMS II ($r = 0.3651$) state. The imaginary components are negligible (on average less than 0.02) and not shown. (b) Linear entropy-tangle plane. Shown are the theoretical curves for MEMS I (solid line), MEMS II (dashed line), and Werner states (dotted line). Four target MEMS states are indicated by stars; the experimental realizations are shown as squares, typically larger than the error bars. The shaded patches around each target state show the range of tangle (T) and linear entropy (S_L) for 5000 numerically generated density matrices that have at least 0.99 fidelity [26] with the target state.

II curve, the optical path length difference in one arm must be varied from 140 nm. This couples different relative timings to the $|H\rangle H_i$ and $|V\rangle V_i$ states, reducing the coherence between them. For instance, to make the MEMS II state (B) in Fig. 2(a), 140 nm decoherence was used in one arm, 90 nm in the other. Visual inspection of the experimental tomographies in Fig. 2(a) shows very good agreement with the theoretical target states. This is confirmed by calculating the fidelity [26] between the target state ($|t\rangle$) and the measured state ($|m\rangle$): $F(|t\rangle, |m\rangle) = \text{Tr} \frac{P_m P_t}{\sqrt{P_m P_t}} = \frac{1}{2} \text{Tr} (P_m P_t)^2$.

The states (A) and (B) are shown in the S_L - T plane

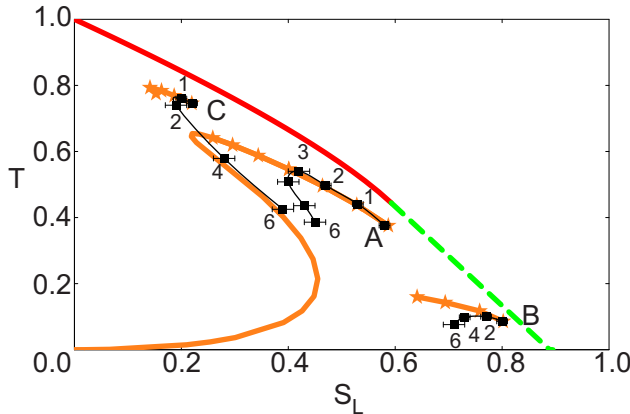


FIG. 3: Concentration data. Shown are concentrations for three initial states, A and B as in Fig. 2, and C. The states are concentrated by preferentially decreasing the value of the $\text{H}\text{V}\text{iH}\text{V}$ element, using partial polarizers in each arm. Shown in squares are the concentrated states, along with the number of glass slips in each arm. The expected concentrated state path, calculated using reference [21], is shown with stars. The concentrated states agree with theory for small numbers of glass slips, but as more slips are used, the state decoheres from multiple reflection effects[31]. Note, however, that even in theory, many stages of Iteration will eventually produce a pure product state (shown as an extension of A's theory curve), due to small errors in the initial M EM S state.

in FIG 2(b), along with other M EM S we created. The states do not hit their S_L - T targets (shown as stars in the figure) within errors, even though the states have very high delties ($\geq 99\%$) with their respective targets. To explore the discrepancy, for each target we numerically generated 5000 density matrices that had at least 0.99 delity with the target density matrix. The S_L and T of the numerically generated states are plotted in Fig. 2(b) as shaded regions surrounding the targets. The fact that these regions are rather large (and overlap with our measured M EM S) explains our results, but is surprising nonetheless. The unexpectedly large size of these patches underscores the great difference in sensitivity between the state measures of delity, tangle and entropy. It indicates that the delity is not very sensitive to a change in S_L and/or T , or conversely, that S_L and T are hypersensitive in comparison. Further investigation is needed to determine whether, for instance, an entanglement measure such as tangle would be superior to delity for benchmarking states used in protocols that require entanglement as a resource.

While our initial goal was to produce states of maximal tangle for a given linear entropy, pure maximally entangled states are generally more useful for quantum information protocols. However, in some cases, weakly entangled mixed states may be the only available resource. It is therefore important to study ways to simultaneously decrease the entropy and increase the entanglement of an ensemble of photon pairs (at the cost

of reducing the size of the ensemble). Recently several such entanglement concentration experiments have been reported, relying on two-photon interference effects [22, 23]. An interesting characteristic of M EM S is that they can be readily concentrated by a "P rocrustean" method of local Iterating [20]. By reducing the $\text{H}\text{V}\text{iH}\text{V}$ element of M EM S state (1) or (2), the outcome will be driven toward the maximally entangled pure state $\text{j}^+ \text{i}^- (\text{H}\text{H}\text{i}+ \text{V}\text{V}\text{i}) = \frac{1}{2}$. We reduce this element by using glass microscope coverslips oriented at Brewster's angle, as indicated in the dotted box in Fig. 1. In the first arm of the experiment, the glass slips are oriented to nearly perfectly transmit vertically polarized photons (transmission probability $T_V = 0.983 \pm 0.001$) while partially reflecting horizontally polarized photons ($T_H = 0.748 \pm 0.001$). In the second arm, an equal number of slips are oriented so that horizontally polarized photons are transmitted with near unit probability and vertically polarized photons are partially reflected.

We concentrated a variety of M EM S. Fig. 3 shows the results for the M EM S I and II states of Fig. 2 and an additional M EM S I (C). As the number of glass slips is increased, the states initially become more like a pure maximally entangled state [31]. For example, in the case of (A), the delity of the initial M EM S with the state $\text{j}^+ \text{i}^-$ is 0.671. When the state is concentrated with three glass slips per arm, the delity with $\text{j}^+ \text{i}^-$ is 0.804, an increase of 20% with 33% of the initial photon pairs surviving the Iterating process.

We now compare the theoreticale ciency of our local Iterating scheme with the interference-based concentration technique of Pan et al. [22], assuming identical initial M EM S states and the same number of photon pairs (the scheme of Yamamoto et al. [23] is unable to distill M EM S). We base our comparisons on the additivity conjecture (e.g. see [32]) of the entanglement of formation (E_F) [25]. Specifically, we will compare the average final E_F (i.e., the E_F of the concentrated state multiplied by the probability of success) per initial pair. The Iterating approach requires only a single photon pair, and succeeds with a probability that depends on the initial state and the amount of Iterating. The interference scheme succeeds with a uniform probability of 50%, but requires two photon pairs. The ideal concentration method depends on the initial state. Table I demonstrates that for certain states, the maximum distillation e ciency from Iteration can exceed that achievable using the interference-based methods [33]. For example, when the initial state is a M EM S with $r = 0.667$, the Iterating technique has a theoreticale ciency nearly twice as high for the same E_F when concentration is successful. Using 3 or 4 slips achieves both higher entanglement of the successful state and better average entanglement yield [33]. (See the final columns of Table I.)

In this letter we have demonstrated a tunable source of high delity M EM S. As a consequence of comparing

Concent. method	Prob. of success	E_F when successful	Ideal E_F per pair	Exp. E_F per pair
Interference	50.0%	0.72	0.18	$< 10^{-5}$
Procrustean				
1 slip	70.0%	0.62	0.44	0.37
2 slips	49.8%	0.69	0.34	0.28
3 slips	35.9%	0.75	0.27	0.21
4 slips	26.1%	0.80	0.21	0.15
5 slips	19.2%	0.84	0.16	0.10

TABLE I: Comparison of efficiencies of interference-based concentration [22] and Procrustean Itering, for an initial MEMS state with $r = 0.667$ and $E_F = 0.550$. In both schemes, we assume the ideal case, i.e., no loss and perfect detector efficiency. In assuming the no-loss condition in our Itering scheme, we normalize the transmission coefficients to $T_H = 0.748 = 0.983$ and $T_V = 1$. In the interference concentration scheme, two identical pairs are needed for concentration. Present technological limitations restrict this to less than 0.005% of the produced coincidence counts (estimated from the 2-fold and 4-fold coincidence data reported in [22]), which is not included in columns 2 or 4, but is in column 5, which gives the actual average entanglement per initial pair. For the Itering technique, we use our measured values of E_F , weighted by the measured pair survival probabilities.

the $T - S_L$ and fidelity values of generated MEMS with the theoretical targets, we identify an unsuspected difference in sensitivity in these state measures. Furthermore, we have implemented a Procrustean Itering technique on several MEMS, realizing a measured efficiency that is well above that achievable using other methods. However, in the limit of very strong Itering, small perturbations in the initial state will eventually dominate the process, yielding only product states (see Fig. 3). In practice, therefore, it may be optimal to combine both methods.

This work was supported by the DCIP postdoctoral Research Fellowship Program, ARDA and the National Science Foundation (Grant number EIA-0121568).

- [1] N. Gisin et al, *Rev. Mod. Phys.* **74**, 145 (2002); Focus Issue on Quantum Cryptography, P. G. Kwiat, ed., *New J. Phys.* **4**, (2002).
- [2] C. H. Bennett et al, *Phys. Rev. Lett.* **70**, 1895 (1993).
- [3] C. H. Bennett and S. J. Wiesner, *Phys. Rev. Lett.* **69**, 2881 (1992).
- [4] S. Bose and V. Vedral, *Phys. Rev. A* **61**, R040101 (2000).
- [5] P. G. Kwiat et al, *Phys. Rev. A* **60**, R773 (1999).
- [6] C. H. Bennett, H. J. Bernstein, S. Popescu, and B. Schumacher, *Phys. Rev. A* **53**, 2046 (1996).
- [7] We adopt the nomenclature suggested in [21], where 'concentration' refers to a 'distillation' process in which both the state purity and the entanglement are increased.
- [8] J. G. Rarity and P. R. Tapster, *Phys. Rev. Lett.* **64**, 2495 (1990).
- [9] P. G. Kwiat et al, *Phys. Rev. Lett.* **75**, 4337 (1995).
- [10] J. Brendel, N. Gisin, W. Tittel, and H. Zbinden,

- Phys. Rev. Lett.* **82**, 2594 (1999).
- [11] C. A. Sackett et al, *Nature* **404**, 256 (2000).
- [12] W. P. Bowen, R. Schnabel, P. K. Lam, and T. C. Ralph, *Phys. Rev. Lett.* **90**, 043601 (2003).
- [13] J. Bao, A. V. Bragaglia, J. K. Furdyna, and R. Merlin, *Nature Materials* **2**, 175 (2003).
- [14] A. G. White, D. F. V. James, P. H. Eberhard, and P. G. Kwiat, *Phys. Rev. Lett.* **83**, 3103 (1999).
- [15] A. G. White, D. F. V. James, W. J. Munro, and P. G. Kwiat, *Phys. Rev. A* **65**, 012301 (2001).
- [16] Y. S. Zhang, Y. F. Huang, C. F. Li, and G. C. Guo, *Phys. Rev. A* **66**, 062315 (2002).
- [17] W. J. Munro, D. F. V. James, A. G. White, and P. G. Kwiat, *Phys. Rev. A* **64**, R030302 (2001).
- [18] Note that for certain entanglement and mixedness parameterizations, the Werner states are the maximally entangled mixed states [24].
- [19] P. G. Kwiat et al, in *Proc. of the 6th Int. Conf. on Quant. Comm., Meas. and Comp.*, J. H. Shapiro and O. Hirota, eds. (Rinton Press, 2003) 117; also quant-ph/0303040 (2003).
- [20] P. G. Kwiat, S. Barraza-Lopez, A. Stefanov, and N. Gisin, *Nature* **409**, 1014 (2001).
- [21] R. T. Thew and W. J. Munro, *Phys. Rev. A* **63**, R030302 (2001).
- [22] J. W. Pan, C. Simon, C. Bruckner, and A. Zeilinger, *Nature* **410**, 1067 (2001); J. W. Pan et al, *Nature* **423** 417 (2003); Z. Zhao et al, *Phys. Rev. Lett.* **90** 207901 (2003).
- [23] T. Yamamoto, M. Koashi, S. K. Ozdemir, and N. Imoto, *Nature* **421**, 343 (2003).
- [24] T. C. White et al, *Phys. Rev. A* **67**, 022110 (2003).
- [25] W. K. Wootters, *Phys. Rev. Lett.* **80**, 2245 (1998); V. Corman and J. Kundu and W. K. Wootters, *Phys. Rev. A* **61**, 052306 (2000).
- [26] R. Jozsa, *J. Mod. Optics* **41**, 2315 (1994).
- [27] D. F. V. James, P. G. Kwiat, W. J. Munro, and A. G. White, *Phys. Rev. A* **64**, 052312 (2001).
- [28] The optical path length difference of the decoherers is not generally exactly 140°, causing an extra phase on the off-diagonal elements. The phase is set to zero by slightly tipping one of the decoherers about its vertical axis.
- [29] A. J. Berglund, *Doctoral Thesis*, also quant-ph/0010001 (2000); N. A. Peters et al, submitted to *J. Quant. Inf. Comp.* (2003).
- [30] M. Barbieri, F. De Martini, G. Di Natale, and P. Mataloni, quant-ph/0303018 (2003); G. Di Natale, F. De Martini, M. Barbieri, and P. Mataloni, quant-ph/0307204 (2003).
- [31] Note that the state actually decoheres when more than a few glass slips are used. We believe that this decoherence is due to multiple reflections between individual glass slips, and between the front and rear surfaces of each slip. The multiple reflections temporally separate the reflected polarization from the transmitted polarization, in the same way that the quartz decoherers do. Because the glass slips partially polarize in the H-V basis, they cause decoherence in that basis.
- [32] P. W. Shor, quant-ph/0305035 p. 20 (2003).
- [33] In practice, because it is very difficult to produce simultaneous pairs of photons, the Iteration technique is much more efficient, e.g., where typically 20% of our incident ensemble of pairs survived, less than 0.005% survive in the two-photon schemes of [22].